TransCom model simulations of hourly atmospheric CO_2: Analysis of synoptic-scale variations for the period 2002–2003

P. K. Patra,[1] R. M. Law,[2] W. Peters,[3,4] C. Rödenbeck,[5] M. Takigawa,[1] C. Aulagnier,[6] I. Baker,[7] D. J. Bergmann,[8] P. Bousquet,[6] J. Brandt,[9] L. Bruhwiler,[3] P. J. Cameron-Smith,[8] J. H. Christensen,[9] F. Delage,[6] A. S. Denning,[7] S. Fan,[10] C. Geels,[9] S. Houweling,[11,12] R. Imasu,[13] U. Karstens,[5,14] S. R. Kawa,[15] J. Kleist,[16] M. C. Krol,[4,12] S.-J. Lin,[10] R. Lokupitiya,[7] T. Maki,[17] S. Maksyutov,[1,18] Y. Niwa,[13] R. Onishi,[19] N. Parazoo,[7] G. Pieterse,[11,20,21] L. Rivier,[6] M. Satoh,[1,13] S. Serrar,[22] S. Taguchi,[23] R. Vautard,[6] A. T. Vermeulen,[20] and Z. Zhu[24]

Received 6 August 2007; revised 22 June 2008; accepted 31 July 2008; published 26 November 2008.

[1] The ability to reliably estimate CO_2 fluxes from current in situ atmospheric CO_2 measurements and future satellite CO_2 measurements is dependent on transport model performance at synoptic and shorter timescales. The TransCom continuous experiment was designed to evaluate the performance of forward transport model simulations at hourly, daily, and synoptic timescales, and we focus on the latter two in this paper. Twenty-five transport models or model variants submitted hourly time series of nine predetermined tracers (seven for CO_2) at 280 locations. We extracted synoptic-scale variability from daily averaged CO_2 time series using a digital filter and analyzed the results by comparing them to atmospheric measurements at 35 locations. The correlations between modeled and observed synoptic CO_2 variabilities were almost always largest with zero time lag and statistically significant for most models and most locations. Generally, the model results using diurnally varying land fluxes were closer to the observations compared to those obtained using monthly mean or daily average fluxes, and winter was often better simulated than summer. Model results at higher spatial resolution compared better with observations, mostly because these models were able to sample closer to the measurement site location. The amplitude and correlation of model-data variability is strongly model and season dependent. Overall similarity in modeled synoptic CO_2 variability suggests that the first-order transport mechanisms are fairly well parameterized in the models, and no clear distinction was found between the meteorological analyses in capturing the synoptic-scale dynamics.

Citation: Patra, P. K., et al. (2008), TransCom model simulations of hourly atmospheric CO_2: Analysis of synoptic-scale variations for the period 2002–2003, *Global Biogeochem. Cycles*, *22*, GB4013, doi:10.1029/2007GB003081.

[1]Frontier Research Center for Global Change, JAMSTEC, Yokohama, Japan.
[2]CSIRO Marine and Atmospheric Research, Aspendale, Victoria, Australia.
[3]Earth Systems Research Laboratory, NOAA, Boulder, Colorado, USA.
[4]Department of Meteorology and Air Quality, Wageningen University and Research Center, Wageningen, Netherlands.
[5]Max-Planck-Institute for Biogeochemistry, Jena, Germany.
[6]Laboratoire des Sciences du Climat et de l'Environnement, IPSL, CEA Saclay, UVSQ, CNRS, Gif Sur Yvette, France.
[7]Department of Atmospheric Science, Colorado State University, Fort Collins, Colorado, USA.
[8]Lawrence Livermore National Laboratory, Livermore, California, USA.
[9]National Environmental Research Institute, Department of Atmospheric Environment, University of Aarhus, Roskilde, Denmark.
[10]Geophysical Fluid Dynamics Laboratory, NOAA, Princeton, New Jersey, USA.
[11]Institute for Marine and Atmospheric Research, Utrecht, Netherlands.
[12]Netherlands Institute for Space Research, University Utrecht, Utrecht, Netherlands.
[13]Center for Climate System Research, University of Tokyo, Chiba, Japan.
[14]Max-Planck-Institute for Meteorology, Hamburg, Germany.
[15]NASA Goddard Space Flight Center, Greenbelt, Maryland, USA.
[16]Privacy Networks, Fort Collins, Colorado, USA.
[17]Atmospheric Environment Division, Japan Meteorological Agency, Tokyo, Japan.
[18]Center for Global Environmental Research, National Institute for Environmental Studies, Tsukuba, Japan.
[19]Earth Simulator Center, JAMSTEC, Yokohama, Japan.
[20]Energy Research Centre of the Netherlands, Petten, Netherlands.
[21]Now at TNO Science and Industry, Eindhoven, Netherlands.
[22]European Centre for Medium-range Weather Forecasts, Reading, UK.
[23]National Institute of Advanced Industrial Science and Technology, Tsukuba, Japan.
[24]Science Systems and Applications Incorporated, Lanham, Maryland, USA.

0886-6236/08/2007GB003081$12.00

1. Introduction

[2] The ability to predict atmospheric CO_2 concentrations into the future depends on our understanding of carbon exchange with the biosphere and ocean. Continental-scale carbon fluxes have been estimated from monthly or annual mean atmospheric CO_2 measurements [e.g., *Gurney et al.*, 2002] using atmospheric transport models. With the availability of more observations with higher temporal resolution, as well as increased computing facilities, there have been several independent attempts to derive fluxes of CO_2 at daily to weekly timescales and/or increased spatial resolution with realistic meteorology [*Law et al.*, 2002, 2004; *Rödenbeck et al.*, 2003; *Peylin et al.*, 2005; *Patra et al.*, 2005; *Rödenbeck*, 2005; *Peters et al.*, 2005]. In the atmospheric phenomena, an overall correspondence is observed between the temporal scales of subdaily, synoptic and annual with the spatial scales of local, regional, interhemispheric transport, respectively. For daily to weekly timescales, the CO_2 concentration footprint extends over $\sim 10^4$ km^2 to $\sim 10^6$ km^2 [*Gloor et al.*, 2001; *Karstens et al.*, 2006]. Thus, a match between the time resolution in the observations used and the spatial resolution of flux inversion regions is required for robust determination of sources/sinks. To estimate CO_2 fluxes at these spatial scales we need at least daily weekly observations and the ability to simulate these accurately. Any error in simulated CO_2 due to misrepresentation of synoptic-scale weather patterns in forward transport modeling would result in biases in regional surface flux derivation by inverse modeling. The requirement to accurately simulate synoptic variations in CO_2 has also been recently noted by *Corbin et al.* [2008] who found that frontal passages had the potential to bias CO_2 flux estimates if sampling time is not accounted for when using future CO_2 satellite measurements in atmospheric inversions.

[3] Some attempts have been made to simulate high-frequency variability in CO_2 using regional and global atmospheric models. These analyses generally suggest that the forward models do capture certain features in observed CO_2 time series. At the continental sites such as Wisconsin tower and in Europe, both the regional-local transport and hourly daily flux variability are found to be important factors for simulating high-frequency variability in CO_2 [*Geels et al.*, 2004, 2007; *Wang et al.*, 2007]. At a remote site in the central Pacific, daily CO_2 variability is found to be controlled by long-range transport [*Wada et al.*, 2007], probably because their study used monthly mean land and ocean fluxes. These results on CO_2 variability are region-specific, on the basis of one or a few transport models and limited in surface flux variety.

[4] In this study, we attempt to analyze daily weekly variations in simulated CO_2 at a variety of measurement stations, e.g., continental, coastal, mountain, and remote/marine, by comparing the model simulations to data from several observational groups worldwide. Forward transport simulations from 25 models and model variants are used to understand differences between the models and to draw overall conclusions regarding the role of model resolution, sampling methods/grid selection, and surface fluxes on CO_2 concentrations. We also discuss the useful model skills revealed from this experiment. The simulations were coordinated through the TransCom group and form an extension to their earlier transport model comparison and CO_2 inversion work [e.g., *Law et al.*, 1996; *Gurney et al.*, 2002]. This paper is a companion to *Law et al.* [2008] (L08) which analyzed diurnal variations in the same set of model simulations presented here.

2. Experimental Details

[5] The experiment is described by L08 and full details are given in the experimental protocol [*Law et al.*, 2006]. Briefly, transport models are run for the 2002–2003 period, following 2 years of spin-up, using nine prescribed surface fluxes (seven for CO_2, plus SF_6 and Radon-222). Three components of surface CO_2 flux are used as detailed by L08: (1) anthropogenic emissions with annual total emission of 6.6 Pg-C a^{-1}, constant throughout the year [*Olivier and Berdowski*, 2001] (FOS), (2) monthly varying ocean exchange with net uptake of 1.64 Pg-C a^{-1} (*Takahashi et al.* [2002], revision 1) (OCN), and (3) five variants of annually balanced terrestrial biosphere exchange from Simple Biosphere Model (SiB, version 3.0; hourly, daily, and monthly means) [*Baker et al.*, 2007] and Carnegie-Ames-Stanford-Approach (CASA; monthly means) [*Randerson et al.*, 1997] (LND). The diurnal variation in the CASA fluxes (CASA-3hr) is imposed by distributing the monthly net primary production and respiration on the basis of solar insolation and surface temperature, respectively, corresponding to the years 2002 and 2003 [*Olsen and Randerson*, 2004] using sunlight and temperature from the European Centre for Medium range Weather Forecasting (ECMWF) archive. The SiB3 model output is based on a fully process based ecosystem model at hourly time intervals [*Baker et al.*, 2007]. While the biospheric fluxes were input to the transport models with (hourly or 3-hourly interval) and without (daily or monthly averages) diurnal variations, the integrated monthly fluxes and monthly mean values were the same for both SiB and CASA models separately. Here we mostly present results based on model simulations utilizing the diurnally varying terrestrial biosphere fluxes, namely, CASA-3hr and SiB-hr. Concentrations from the three flux components are added to construct atmospheric CO_2 concentrations and then compared to observations.

[6] Twenty-five transport models or model variants (Table 1) performed the simulations and submitted hourly atmospheric concentrations at 280 surface, tower and aircraft measurement locations (3-hourly for IFS.ECMWF). Note that DEHM and IFS simulations were only performed for FOS, OCN and CASA-3hr fluxes only, and are therefore not included in the later part of the analysis (after section 3.2) where results using both CASA and SiB fluxes are discussed. All chemistry-transport models (CTMs; offline dynamics) are driven by analyzed meteorological fields corresponding to the years 2002 and 2003 (see Table 1 for the data source). The tracer simulations using online dynamics, based on general circulation models (GCMs), are carried out in nudged-meteorology mode, where the GCM calculated horizontal winds (U, V) and sometimes temperature (T) are modified toward analyzed meteorology with

Table 1. List of Transport Models Participating in TransCom Intercomparison Experiment of Hourly Atmospheric CO_2

Serial Number	Model Name Institution[a]	Resolution		Meteorology[d]
		Horizontal[b]	Vertical[c]	
1	AM2.GFDL	2.5 × 2.0°	24η	NCEP; *U*, *V*
2	AM2t.GFDL	2.5 × 2.0°	24η	NCEP; *U*, *V*, *T*
3	CCAM.CSIRO	~220 km	18σ	NCEP; *U*, *V*
4	CCSR_NIES1.FRCGC	T42 (~2.9°)	32σ	NCEP; *U*, *V*, *T*
5	CCSR_NIES2.FRCGC	T106 (~1.2°)	32σ	NCEP; *U*, *V*, *T*
5a[e]	CCSR_NIES2lrf.FRCGC	T106 (~1.2°)	32σ	NCEP; *U*, *V*, *T*
6	CDTM.JMA	2.5 × 2.5°	32η	JRA-25/JMA
7	*CHIMERE.LSCE*	0.5 × 0.5°	20σ	MM5/ECMWF
8	*COMET.ECN*	1.0 × 1.0°	2	ECMWF
9	*DEHM.NERI*	50–150 km	20σ	MM5/ECMWF
10	IFS.ECMWF	T159 (~1.2°)	60η	ECMWF, T511; *U*, *V*
11	IMPACT.LLNL	2.5 × 2.0°	55η	NASA/GSFC/GEOS4
12	LMDZ.LSCE	3.75 × 2.5°	19η	LMDZ/ECMWF
13	LMDZ_THERM.LSCE	3.75 × 2.5°	38η	LMDZ/ECMWF
14	NICAM.CCSR_FRCGC	~240 km	54z*	NCEP; *U*, *V*, *T*
15	NIES05.NIES.ESC	1.0 × 1.0°	47σ	NCEP
16	PCTM.CSU	1.25 × 1.0°	25η	NASA/GSFC/GEOS4
17	PCTM.GSFC	2.5 × 2.0°	25η	NASA/GSFC/GEOS4
18	*REMO.MPIBGC*	0.5 × 0.5°	20η	ECMWF[f]
19	STAG.AIST	1.12 × 1.12°	60η	ECMWF
20	STAGN.AIST	1.9 × 1.9°	28σ	NCEP
21	TM3_fg.MPIBGC	3.8 × 5.0°	19σ	NCEP
22	TM3_vfg.MPIBGC	1.9 × 1.9°	28σ	NCEP
23	TM5_glb3x2.ESRL	3.0 × 2.0°	25η	ECMWF
24[g]	TM5_nam1x1.ESRL	3.0 × 2.0°	25η	ECMWF
25[g]	TM5_eur1x1.SRON	3.0 × 2.0°	25η	ECMWF

[a]See authors' affiliations for full institute name. Four models, 7–9 and 18 are run over regional domains and identified in italics. Bold indicates general circulation models (GCMs)-based online models, and the rest are offline CTMs run over global domain (see section 2).

[b]The horizontal model grids are given as longitude × latitude, linear distance, or spectral truncation (*T*).

[c]Vertical grid systems are mainly σ (pressure normalized by surface pressure) or η (hybrid sigma-pressure). NICAM uses terrain (z_s) following vertical coordinate $z^* = z_t(z - z_s)/(z_t - z_s)$; z_t is model top height.

[d]Sources; parameters used in online models. *U*, *V*, and *T* are listed only for the online models, where the GCM transport was nudged to analyzed meteorology.

[e]This model is run as a special case at T106 horizontal model resolution using the surface fluxes at T42 resolution to quantify relative impacts of both on simulation of atmospheric CO_2.

[f]Serial number 18 is run in forecast mode with respect to meteorology in combination with continuous tracer transport.

[g]These two TM5 versions are run at 1 × 1 degree horizontal resolution over North America (nam1 × 1) and Europe (eur1 × 1).

order of days relaxation times. This enables a realistic representation of synoptic meteorology in the forward tracer transport.

[7] Additional model output was submitted for a subset of 100 stations comprising meteorological data, surface fluxes and concentrations for all levels to about 500 hPa. One application of the profile data is the analysis of CO_2 data at mountain sites, where the selection of the appropriate vertical model level remains challenging for coarse-resolution models [*Geels et al.*, 2007; L08]. Some model (TM5s, LMDZs, and REMO) results are submitted after interpolation to the station locations. Others have selected the nearest horizontal model grid to the observation location for sampling (land and ocean grids for some coastal sites), but the choice of vertical sampling location varied widely.

2.1. In Situ Observation Network

[8] We will analyze synoptic-scale variations in atmospheric CO_2 using daily average observations calculated from continuous in situ measurements and model output. Various organizations independently operate these 35 measurement sites (see Table 2) and made continuous observations of CO_2 every few minutes (i.e., high frequency) for the analysis period of 2002–2003. We obtained hourly averaged data from the WMO World Data Centre for Greenhouse Gases (Japan Meteorological Agency, Tokyo, 2007, data available at http://gaw.kishou.go.jp) database or through personal communication. Although most observations are on the World Meteorological Organization (WMO) CO_2 scale, the intercalibration of standard gases is not critical for this study because we will be dealing with model-data comparison in a relative sense (variability only) as described in section 2.2. Figure 1 shows the locations of observation stations used in this work and the sampling location corresponding to different transport models. Generally, the largest scatter in the location where models are sampled is found at coastal stations (e.g., BHD, CGO, RYO, and WES) because the experimental protocol requested that two points be submitted to represent these sites, one location that was predominantly land and another that was predominantly ocean. The stations can be broadly categorized as continental (mainly under the influence of land fluxes), coastal (under the influence of land and ocean flux), remote/oceanic (dominated by ocean flux) or mountain (continental but at high elevation).

Table 2. Details of Data Sources and Responsible Organizations for Taking Measurements at Different Continuous CO_2 Monitoring Stations[a]

Station Name	Managing Institute	Data Source
ALT	Meteorological Services Canada/Environment Canada	Doug Worthy (personal communication, 2006)
AMS, MHD	Laboratoire des Sciences du Climat et l'Environnement, France	*Gaudry et al.* [1990] and *Biraud et al.* [2002]
AMY	Korea Meteorological Administration	*Kim and Park* [2006]
BHD	National Institute of Water and Atmospheric Research, New Zealand	A. Gomez (personal communication, 2006)
BRW, MLO, SMO, SPO	Global Monitoring Division, ESRL/NOAA, USA	*Conway et al.* [1994]
CBW; data at two levels	Energy Research Centre of the Netherlands	A. Vermeulen (personal communication, 2006)
CGO	Commonwealth Scientific and Industrial Research Organization, Australia	*Langenfelds et al.* [2002]
CMN	Institute of Atmospheric Sciences and Climate, Italy	R. Santaguida (personal communication, 2006)
CPT	South African Weather Service	*Brunke et al.* [2004]
DDR	Center for Environmental Science in Saitama, Japan	*Muto* [2006]
DEU, NGL, ZGP, SCH, WES, ZGT	Umweltbundesamt, Air Monitoring Network of the Federal Environmental Agency, Germany	*Uhse et al.* [2006]
HUN; data at two levels	Hungarian Meteorological Service	*Haszpra* [2006] and *Haszpra et al.* [2001]
LEF; data at three levels	Global Monitoring Division, ESRL/NOAA, USA	*Bakwin et al.* [1995] and Arlyn Andrews (personal communication, 2006).
MKW	Aichi Environmental Research Center, Japan	*Iwata* [2006]
MNM, RYO, YON	Japan Meteorological Agency	*Sasaki* [2006] and *Tsutsumi et al.* [2006]
PAL	Finnish Meteorological Institute	*Hatakka* [2006]
PRS	Italian Electrical Experimental Center, CESI RICERCA	*Martinotti et al.* [2006]
SYO	National Institute of Polar Research and Tohoku University, Japan	*Morimoto et al.* [2000]
TKY	National Institute of Advanced Industrial Science and Technology, Japan	*Murayama et al.* [2006]
WLG	Chinese Acadamy of Meteorological Sciences	*Zhou et al.* [2003]

[a]See Figure 1 for locations.

2.2. Extraction of Synoptic Variations in CO_2

[9] Atmospheric CO_2 time series contain mixed signals of the seasonal cycle, synoptic variations, diurnal cycle and long-term growth rate. We fit all the data using a digital filtering technique [*Nakazawa et al.*, 1997] which uses three Fourier harmonics and Butterworth filters of order 16 and 26 with a cutoff frequency of 24 months to represent a smooth seasonal cycle and long-term trend, respectively. The filter is applied to the 2-year (2002–2003) simulated period. For sites with a large diurnal cycle (e.g., Neuglobsow shown in Figure 2) we tested the sensitivity of the filter to daily averages using all 24-hourly CO_2 data or afternoon data only (13–16 local time (LT)), having first converted all model results and observations (as applicable) to LT. We define 1–10 day variations in atmospheric CO_2 as synoptic-scale variations, derived by subtracting the fitted curve from the original daily average time series as depicted in Figure 2b. The example demonstrates that the derived synoptic-scale variations are fairly independent of whether all data or afternoon only data were used. This is because the synoptic variability is generally transport dominated; the major cause for synoptic variations in CO_2 or other tracers such as water vapor is the direction of the winds which bring tracer rich or depleted air masses to the observing stations from their source or sink regions, respectively, and the height of the planetary boundary layer (PBL). During a low-pressure event the PBL is thicker and source ventilation is quicker resulting in lower CO_2 concentrations in comparison with average meteorological conditions. The situation is opposite under the influence of a high-pressure system. Note here that the fitting of data at noncontinental sites (coastal, remote, or mountain) is less ambiguous. For example, at Alert the difference between the fitted curves by selecting all data and afternoon only values is negligible (not shown) and the synoptic variations are also relatively less noisy compared with those shown in Figure 2b.

3. Results and Discussion

[10] There are many possible approaches to analyzing the synoptic-scale variability found in the model simulations and observations. Here we have chosen to present a comparison between model and observations at a single site for a relatively short period to illustrate typical model behavior. We then provide an overview of the behavior across all sites by correlating modeled and observed synoptic variability. The model performance is further assessed for separate seasons and different classes of sampling location. We also assess whether comparisons with the observations can be improved by using the ensemble model mean (constructed by averaging multimodel time series). If we think of a

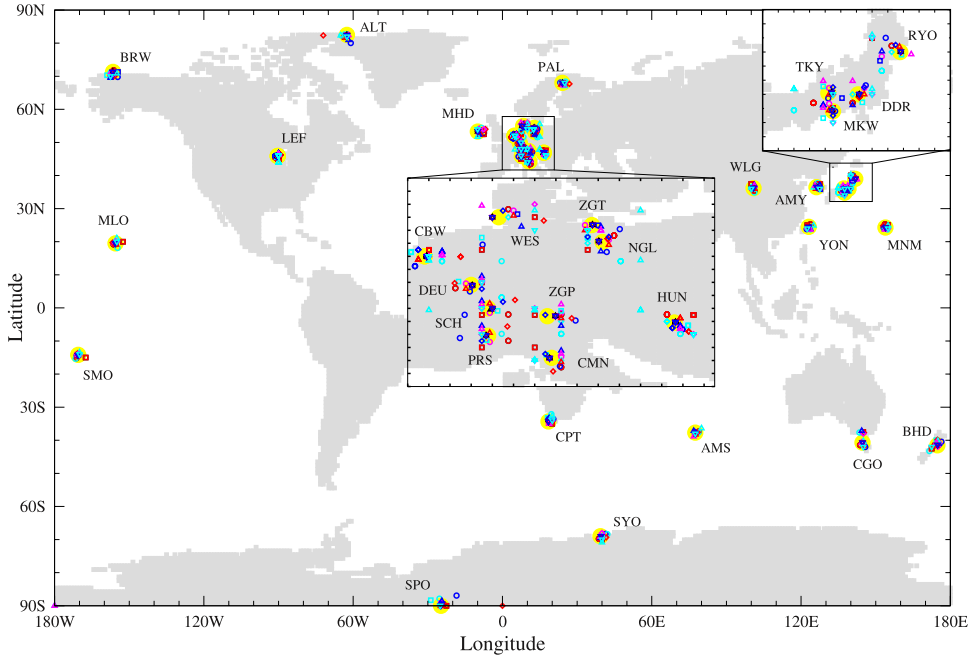

Figure 1. Observation station locations (large yellow symbols) and model sampling locations (small symbols). Europe and Japan are expanded to accommodate the higher density of sites in these regions. Observation data are either taken from the WMO World Data Centre for Greenhouse Gases, (Japan Meteorological Agency, Tokyo, 2007, data available at http://gaw.kishou.go.jp) or obtained through personal contacts (see Table 2 for details).

model simulation as composed of the signal that we wish to model plus model-generated noise, we might anticipate that the ensemble mean will reduce the noise component while maintaining the signal component.

3.1. Comparison With Tall Tower Observations

[11] Most of the high-frequency CO_2 measurements are made near the surface, and a few of the sites considered here (e.g., CBW, HUN, and LEF) record CO_2 data at several vertical layers up to about 400 m using tall towers. One of the tallest towers (447 m) for measuring CO_2 and other atmospheric minor constituents is operated at LEF [*Bakwin et al.*, 1995]. Figure 3 shows the observed time series of daily CO_2 variabilities in comparison with model simulations at this site. We also show rainfall, outgoing long-wave radiation (OLR) and CASA-3hr CO_2 fluxes (Figure 3a). Low OLR indicates cloud cover in the presence of low-pressure systems and is generally associated with rainfall events. The CASA-3hr fluxes are generated from modeled monthly mean fluxes using meteorological parameters (solar radiation influx and temperature) and thus exhibit very good correspondence with OLR, but do not include the effect of rainfall. Under cloudy conditions net primary production (NPP) is reduced and sometimes respiratory release exceeds NPP (net positive CO_2 flux), in contrast to the strongly negative fluxes under sunny conditions (high OLR). However, the observed and modeled CO_2 time series are not so straightforward to interpret as the synoptic variations in both meteorology and fluxes control the variability in CO_2. Figure 3b shows the observed CO_2 synoptic variability at two tower levels (76 and 244 m) and Figures 3c–3f show modeled CO_2 synoptic variability. The model results shown generally represent the 76 m level, but in two cases (CCAM and LMDZ_THERM) the 244 m level submission (corresponding to their model level 2) was used as this provided a better agreement to the observations. At lower levels these models substantially overestimated the magnitude of synoptic variations. This illustrates the difficulty of appropriately matching a given sampling height to a model level.

[12] Low-pressure systems passed over LEF site on 8 and 10 July and 3–6 August followed by high-pressure systems during 12–16 July and 8–11 August, respectively (Figure 3a). All the models consistently simulated high CO_2 values during the overcast condition (low OLR), followed by prolonged low CO_2 values during the clear-sky days, in agreement with the observations. This agreement with the observations can be quantified by correlating the modeled daily variations with those observed. For the time period plotted, the correlations range from 0.45 to 0.84, with 16 out of 22 models giving a correlation higher than 0.7. The mean correlation is 0.73 (range: 0.45 to 0.84), and the standard deviation (SD; 1σ) of modeled daily CO_2 variability ranged from 5.35 to 9.75 with a mean of 7.33 ppm, about 11% lower than observed (8.24 ppm). The ensemble model mean for this period gives a correlation with the observations of 0.85, which is slightly larger than any individual model for CASA-3hr flux. The standard deviation is 25% lower than observed, which is consistent with the ensemble mean reducing the noise component of an individual model

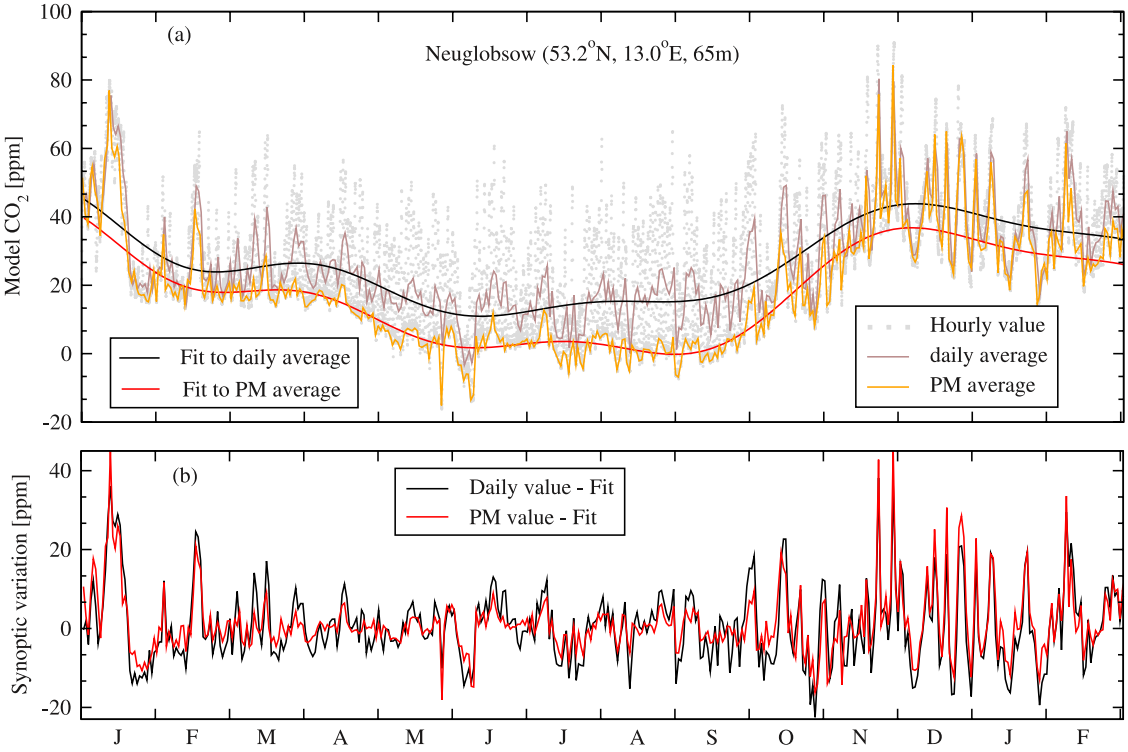

Figure 2. (a) Hourly modeled CO_2 concentration (gray dots) at Neuglobsow from the CCSR_NIES2.FRCGC transport model using FOS+OCN+SiB-hr fluxes, daily averaged CO_2 (brown line), PM average (13–16 LT) CO_2 (orange line), and the digital filter fit to the daily average CO_2 (black line) and PM average CO_2 concentrations (red line). (b) Synoptic-scale variations in CO_2 defined as the difference between the raw data and the fitted data for the daily averaged CO_2 (black line) and PM average CO_2 (red line).

simulation. The ensemble model mean across all sites is discussed in section 3.3. Using SiB-hr flux, the correlations and SDs ranged from 0.31 to 0.78 and from 4.83 to 9.62 ppm, respectively, with average values 0.56 and 6.42 ppm.

[13] The ensemble average CO_2 variability (both phase and amplitude) is in better agreement with observations at LEF when using CASA-3hr as compared to SiB-hr (variability 1σ = 6.57 ppm, correlation = 0.54). However, this result does not appear to be typical of all continental sites in summer as we discuss later (section 3.5). The CASA-3hr fluxes have larger day-to-day variations than the SiB-hr fluxes and this suggests that during the July–August period these flux variations are the dominating factor in controlling CO_2 concentration variability at this site. There is also evidence that the temporal resolution of the land fluxes has an important impact on the quality of the simulated CO_2. For example, the correlations at the LEF site are systematically higher by about 0.3 for all models when CASA-3hr and SiB-hr fluxes are used compared to the use of monthly averaged fluxes from CASA and SiB for the period of 2002–2003. Further analysis, beyond the scope of this paper, is needed to identify the sensitivity of biospheric model parameters to the meteorological conditions, ideally under the ongoing projects like CarboEurope and North American Carbon Project (NACP).

3.2. Correlations Between Observed and Modeled CO_2 Variations

[14] Figure 4 shows the correlation (r) between daily averaged modeled and observed CO_2 time series at all stations for the period of 2002–2003. Our analysis suggests that all the models simulate the observed synoptic-scale variations fairly well ($r > 0.3$, n = 730) at most stations. The larger correlations are obtained at measurement sites where the flux signals of different flux types (fossil fuel burning, land ecosystem and ocean exchange) can be distinguished, following the tracks of synoptic dynamical systems. How distinctly such signals reach a station depends on the transport model resolution, the quality of the model transport and the flux heterogeneity in the vicinity of the site. The high correlations at several coastal sites in Europe are due to the clearly contrasting land and ocean fluxes (with much smaller and less variable fluxes from the ocean). A similar sharp concentration boundary can develop at MNM and YON between the air mass influenced by East and Southeast Asian fluxes and that dominated by West Pacific fluxes. However, if flux distributions are not representative of the observation sites low correlations may be obtained. This can occur when the model sampling location is relatively distant from the observing site (Figure 1) because of coarse model resolution. A few sites in the Japanese main

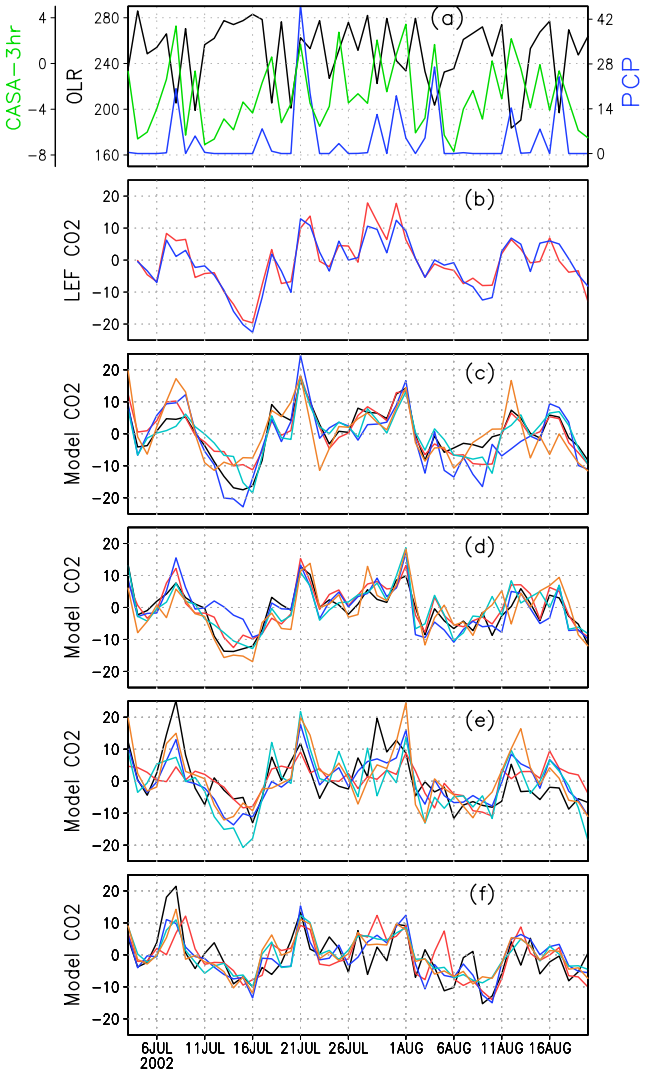

Figure 3. (a) Daily averaged CASA-3hr terrestrial CO_2 fluxes in gC m^{-2} day^{-1} (green line), NCEP interpolated outgoing long-wave radiation, outgoing long-wave radiation in W m^{-2} (black line), and precipitation (PCP) as the Tropical Rainfall Measuring Mission (TRMM) accumulated rainfall in millimeters (blue line). (b) Observed and (c–f) modeled synoptic variations in daily averaged CO_2 (in ppm) at LEF tower (90.3°W, 45.9°N) for 4 July to 20 August 2002. The observed CO_2 is shown at two levels (red line: 76 m, blue line: 244 m). Model simulations are obtained using CASA-3hr+FOS+OCN fluxes and represent the 76 m or 244 m tower height depending on the model. The black, red, blue, cyan, and orange colored lines are for models 1–3, 5, and 6 (Figure 3c); 10–14 (Figure 3d); 15–19 (Figure 3e); and 20–22, 23, and 24 (Figure 3f), respectively. Regional models 7–9 run over Europe domains and models 4 and 25 having common model versions (5 and 25, respectively) are excluded. All daily average CO_2 values are detrended and deseasonalized by subtracting a fitted curve as discussed in section 2.2.

islands (e.g., DDR, MKW, and RYO) are good examples of this case. It may be cautioned here that observations at the DDR site are not regionally representative (close to megacity Tokyo) and data from such sites are not suitable for comparison with coarse-resolution global model results.

[15] Other sites with low correlations (e.g., MLO, AMS, and SPO) are remote from regions with large fluxes and the synoptic variations are typically smaller by several times compared to the continental or coastal sites. In particular, the standard deviation of observed daily average CO_2 variability at AMS, SPO and SYO is 0.27, 0.12 and 0.07 ppm, respectively, similar to the measurement accuracy. The low variability may contribute to the low correlations at these locations but across the remaining sites we did not find a strong relationship between variability and correlation. For the remote sites it is difficult to diagnose whether the small correlations are mostly due to errors in transport of the remote flux signals to the site or due to errors in the nearer ocean fluxes e.g., through the use of monthly flux estimates only.

[16] To check the similarities between model simulations, correlations between the daily averaged CO_2 variabilities from different models have been calculated. These between-model correlations, ranging from 0.48 to 0.74, show better agreement among the model simulations compared to those between observations and the models; correlations averaged over 35 stations are greater by 0.15. This indicates that the first-order transport mechanisms are fairly similar among the models regardless of the meteorological analysis data being used to force the model. The higher model-model correlations are not likely to be caused by systematic error in all model transport because we obtained an improved model-data correlation in the case of ensemble mean model compared to individual models. We also find no discernible systematic differences between the "offline" (driven by analyzed meteorological data only) and "online" (general circulation-based meteorology nudged to analyzed meteorology) transport models. Where discrepancies between models arise, they often result from the different model resolutions used and the consequent variations in how the common set of surface fluxes were represented and where the model grid was sampled to represent each site. Examples are given in later sections.

3.3. On Capturing the Phase of Variability

[17] In addition to testing the statistical significance of the correlations, we have checked the lagged correlation with the observations leading or lagging by up to 5 days for all models and stations. Figure 5 shows the resulting correlations for all global models except IFS (i.e., 20 model variants; averaged across the 35 sites shown in Figure 5a), and for all sites (calculated by averaging the individual model correlations in Figure 5b and by correlating the ensemble model average with observations in Figure 5c). In all the cases (Figure 5a) maximum correlations are obtained at zero time lag, and monotonically decrease with increasing lead-lag. The choice of CASA or SiB as terrestrial biosphere flux does not make any difference to this interpretation. The correlations tend to decrease less rapidly when the observations lag the model compared to when the

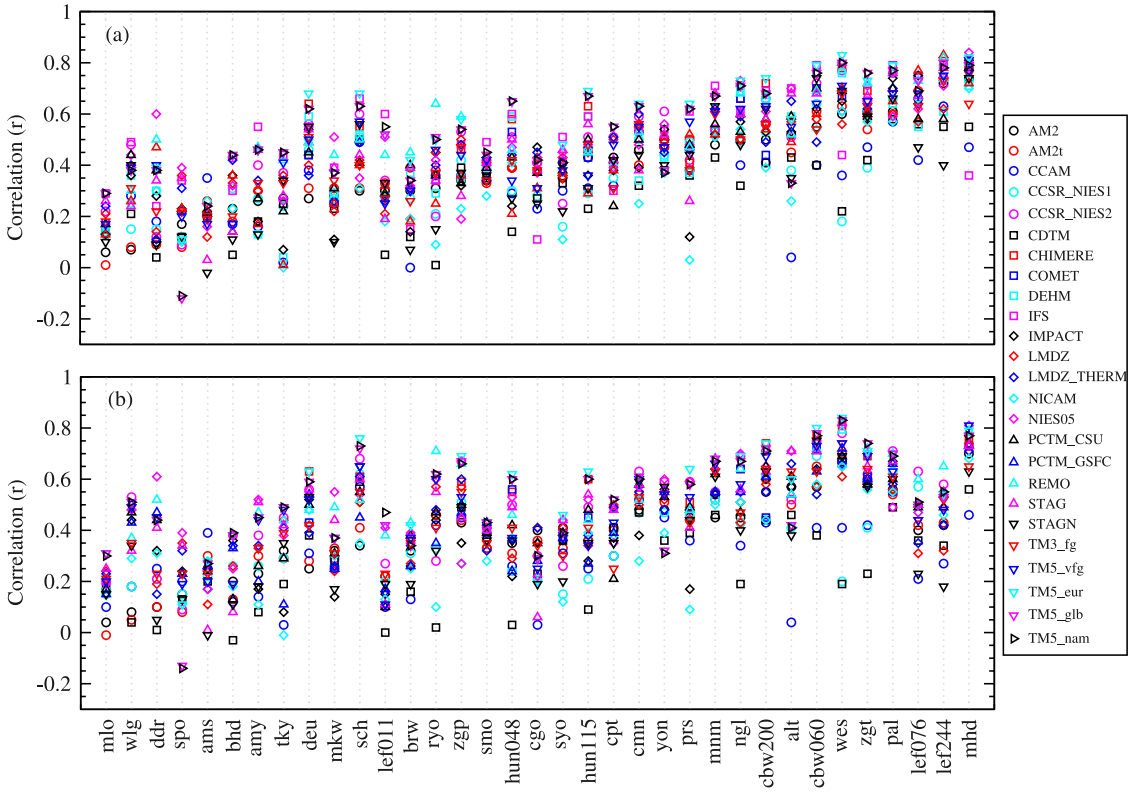

Figure 4. Correlation between daily averaged modeled and observed atmospheric CO_2 concentrations for (a) FOS+OCN+CASA-3hr and (b) FOS+OCN+SiB-hr fluxes. Each model is represented by a different symbol. The sites are ordered from lowest to highest correlation using the results from an arbitrary model in Figure 4a. COMET model results for sites located higher than 300 m are not shown, because this version is not suitable for simulating elevated sites.

observations lead. This is due to the shape of the CO_2 concentration peaks, which tend to rise sharply and drop off slowly on most occasions (refer to Figure 3b for instance). The cause of this skewness in CO_2 peaks is beyond the scope of this study, but a complex mixture of contributions from synoptic changes in transport and biospheric flux is envisaged.

[18] Figure 5a suggests that some models give consistently better correlations than others. The three largest average correlations are produced by TM5s (0.54), NIES05 (0.49), CCSR_NIES2 (0.48) while four models give rather lower correlations than most models (CDTM, NICAM, CCAM, and CCSR_NIES1) among the global models. The regional models are excluded from this list as their station lists do not include southern hemispheric remote sites where the correlations are the lowest. The simplest difference between the models with low and high correlations is coarser and finer horizontal resolution, respectively. The larger correlations for the TM5 model cannot be explained by the finer horizontal resolution only. Other possible explanations are (1) the preprocessing of the ECMWF 6-hourly windfields [*Bregman et al.*, 2003], (2) the use of 3-hourly ECMWF surface fields in resolving the boundary layer dynamics (as is the case for NIES05), and (3) the modification of the vertical tracer slope [*Russell and Lerner*, 1981] when CO_2 is emitted or taken up at the surface. Figure 5b shows that all but two sites (AMY and MKW) peak at zero lag. Thus there is no indication that flux signals are consistently transported to sites too slowly or too quickly. The correlations in Figure 5c are obtained by taking the ensemble model average of the individual model time series. For almost all sites the model ensemble gives higher correlations with the observations compared to the average correlation of individual models shown in Figure 5b. Averaged across all sites the ensemble mean gives a correlation of 0.52 for FOS+OCN+CASA-3hr flux, close to the maximum correlation obtained for any individual model (Figure 5a). It appears that the ensemble mean is successful in reducing some of the noise in individual model simulations, while retaining the major synoptic CO_2 variations that are represented in the observations.

3.4. Relative Amplitude and Phase of Synoptic CO_2 Variability

[19] In addition to capturing the timing of variability (as measured by the correlation), the amplitude of variation is an important factor to simulate and should be included in the evaluation of model performance for simulating the synoptic-scale variations. We calculated the standard deviation from the daily average time series of model simulations and observations and created a normalized standard deviation (NSD) by dividing the model SD by the observed

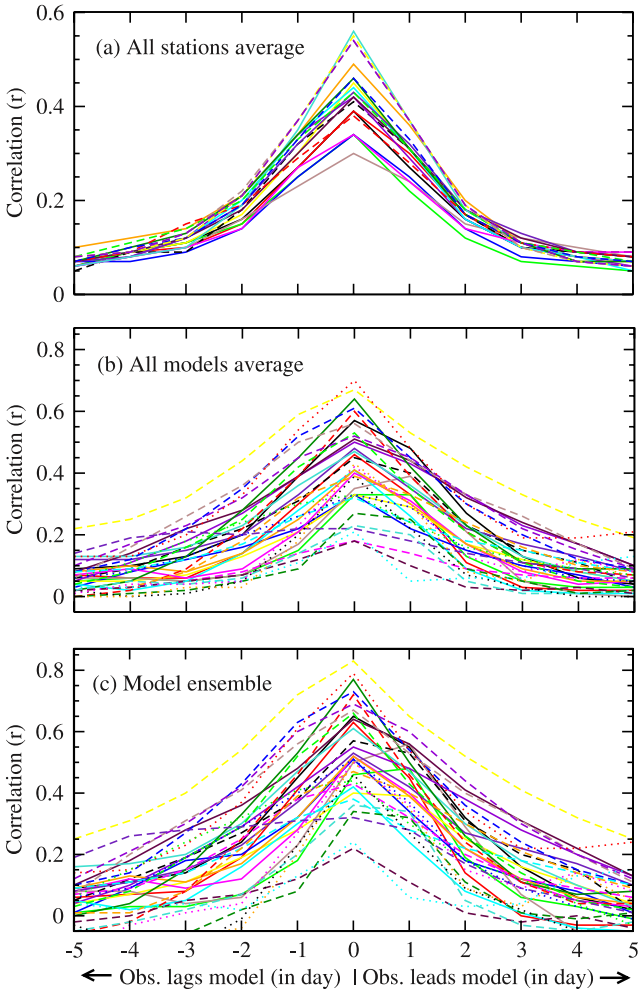

Figure 5. Correlation between modeled and observed daily average CO_2 at different time lags for (a) different models with correlations averaged across sites, (b) different sites with correlations averaged across models, and (c) different sites for the model ensemble average correlated with observations. The model simulation uses the CASA-3hr fluxes for Figure 5a and the SiB hourly fluxes for Figures 5b and 5c, in addition to FOS+OCN. Correlations at MKW and SPO sites only do not peak at 0 lag. Note the different *y* axis range for Figure 5a and Figures 5b and 5c.

SD The NSDs are plotted against correlation using Taylor diagrams [*Taylor*, 2001]. A value of 1 on the linear and polar axis indicates a perfect fit between the measurements and simulations. Figure 6 shows the Taylor diagrams for four groups of sites and for winter and summer separately. Here we have used the CASA-3hr fluxes for the biosphere component but the results are similar for the SiB-hr fluxes, both cases giving NSDs closer to 1 than if monthly mean biosphere fluxes are used. The all-station mean correlation using SiB hourly, daily, and monthly fluxes are 0.42, 0.39 and 0.39, respectively, and the values of NSDs are 1.07, 1.03 and 0.94. This reiterates the importance of diurnally varying fluxes for realistic simulations of synoptic variations in CO_2 and perhaps point to the importance of diurnal correlations in meteorology and CO_2 fluxes. Figure 6 suggests that the models' performance is generally better during the winter than summer at all types of sites; at coastal sites the better performance is primarily in the correlation whereas for remote sites the better result is mainly in the NSD. Such differences in model performance probably arise because of uncertainty in the large biospheric fluxes in summer when the photosynthetic activities are at the highest and the daily mean biosphere flux is a sink, opposite in sign to the fossil emissions. The net land flux may consequently be quite variable in both sign and magnitude leading to the uncertainty in the modeled concentration. During winter, when the fossil fuel and land biosphere fluxes have the same sign and have smaller spatial and temporal variations, the model simulations match better with the observed variabilities.

[20] A comparison of the behavior between site types reveals several salient features:

[21] 1. At mountain sites (Figure 6a) the large range of NSDs may be due in part to the model layers selected to represent these sites; some models selected the surface layer for these sites and consequently have large NSDs. The low NSDs are likely caused by sampling a model level too high in the atmosphere since the surface signals decays with height as revealed by analysis of submitted profile data. NSD close to 1 and highest correlation for all models is obtained at a nonsurface model layer. This "best" layer is usually a lower model layer than that applicable to the station altitude, which is a similar result to that found for the diurnal cycle at mountain sites [L08]. This is a problem associated with coarse vertical resolution in models and their inability to resolve flow associated with mountains. Typical behavior would be that the mountain site samples the free troposphere during nighttime and the upslope winds may bring boundary layer air to the site during the day.

[22] 2. The synoptic-scale CO_2 variations at continental sites located in relatively low altitude and homogeneous terrain are best represented by the transport models. This suggests that the combination of terrestrial biosphere/fossil fuel fluxes and forward transport are fairly realistically modeled over the land in our experiment. However, most models underestimate the NSDs during the summer and only CCAM (1.07), CHIMERE (0.98), STAG (1.02) and REMO (1.04) produced NSD close to 1. During the winter CHIMERE, TM5s, STAG and CCSR_NIES2 showed maximum correlations between the filtered data and model results.

[23] 3. For the coastal sites the agreement between observations and model simulations is seasonally dependent, with winter correlations clearly better than summer ones. This indicates the role of seasonal changes in meteorology. For example, at YON site when the winds are generally from the Asian continent to the Pacific Ocean (winter) the correlations (~0.6) are often found to be twice as large compared to when the wind direction reverses in the summer. This seasonal difference may also arise from the simplicity in fluxes during winter (mainly fossil fuel and biospheric respiration) compared to the summer when the biospheric fluxes (e.g., synoptic variation in photosynthesis)

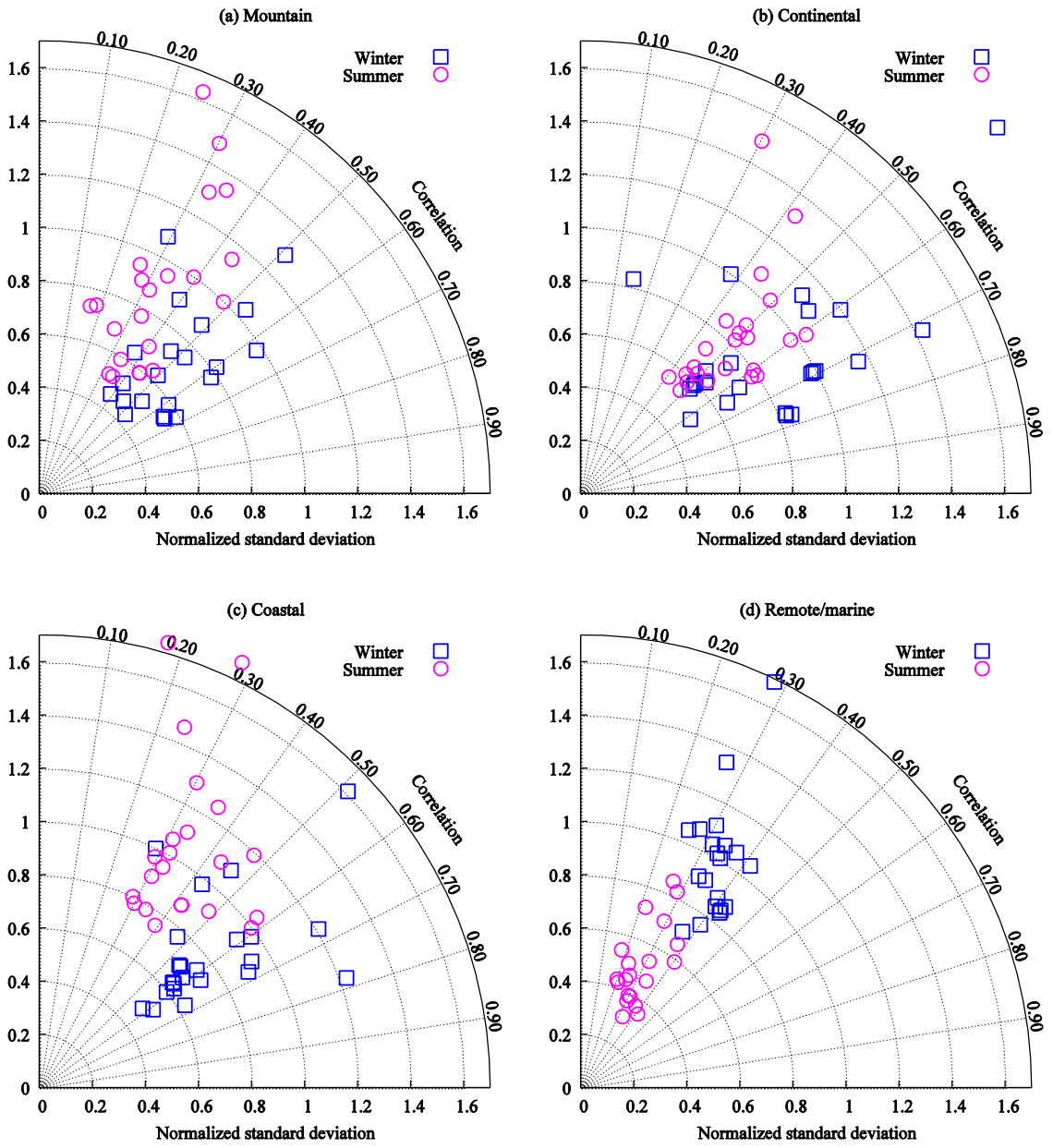

Figure 6. Taylor diagrams showing average correlations and normalized standard deviations (NSD) (1σ; ratio of model to observed standard deviation (SD)) corresponding to four station categories: (a) mountain (CMN, DDR, DEU, PRS, ZGP, SCH, TKY, and WLG), (b) continental (HUN, LEF, MKW, NGL, PAL, and ZGT), (c) coastal (ALT, BHD, BRW, CBW, CGO, CPT, MHD, WES, and YON), and (d) remote/marine (AMS, MNM, MLO, SMO, and SPO) for summer and winter in the period 2002–2003. Winter is defined as December–February in the Northern Hemisphere and June–August in the Southern Hemisphere and vice versa for summer. Each symbol represents average correlation and NSD for each model using FOS+OCN+CASA-3hr fluxes. The NSDs versus $90 \times (1 - r)$ are plotted in these polar diagrams for adopting a linear axis for correlation (r).

are more difficult to model as well as the low oceanic flux frequency (presently of month interval) and magnitude, particularly in the coastal regions which are not covered by the coarse-resolution ($4 \times 5°$) flux maps.

[24] 4. The correlations between observed and modeled CO_2 synoptic variability at remote/marine sites are lowest and do not show prominent seasonality. The NSDs are more realistic in winter than summer when the models underestimate the variability. We investigated this behavior at one site, MNM, and found that the observations show rare occasions with very low CO_2 which can persist for 2–3 days. *Wada et al.* [2007] identified these events as continental in origin and in their test cases for 7 July and 22 August 2001, were able to reproduce the low concentration using the

Table 3. Summary of Correlations and NSDs of Synoptic Variations for Different CO_2 Flux Components (Columns 2–8) and After Combining (Last Five Columns), for Each Season and After Averaging Over All Observation Sites and All Transport Models[a]

	Individual Tracers							After Combining: BIO+FOS+OCN				
Season	SH	SD	SM	CH	CM	FOS	OCN	SH[b]	SD[b]	SM[b]	CH[b]	CM[b]
						Correlations						
Winter	0.37	0.36	0.37	0.46	0.45	0.49	0.09	0.46	0.45	0.46	0.52	0.51
Spring	0.09	0.01	0.01	0.25	0.14	0.35	0.05	0.30	0.23	0.25	0.38	0.33
Summer	0.34	0.27	0.22	0.28	0.09	0.18	0.24	0.41	0.37	0.35	0.36	0.26
Autumn	0.34	0.30	0.32	0.40	0.36	0.39	0.19	0.46	0.45	0.46	0.49	0.47
						NSDs						
Winter	0.94	0.94	0.91	0.59	0.58	0.59	0.20	1.37	1.36	1.35	1.09	1.08
Spring	0.82	0.89	0.78	0.89	0.70	0.57	0.21	1.03	1.03	0.94	1.24	1.00
Summer	0.91	0.88	0.68	0.89	0.62	0.38	0.17	1.10	1.03	0.80	1.06	0.70
Autumn	0.70	0.65	0.59	0.65	0.46	0.46	0.16	1.02	0.95	0.90	1.00	0.81

[a]The abbreviated tracer names are SH, SD, and SM for SiB hourly, daily, and monthly fluxes; and CH and CM for CASA 3-hourly and monthly fluxes, respectively. NSD is normalized standard deviation.
[b]These columns are for FOS+OCN+BIO combined fluxes.

STAG model with FOS+OCN+CASA-mon fluxes. This is in contrast to our results where any low-CO_2 events due to negative biosphere fluxes are significantly moderated by positive contributions from fossil emissions. Another possible reason for the difficulty in modeling remote sites may be the use of monthly, climatological ocean fluxes. Recent analysis shows the presence of a greater variability in sea-air CO_2 fluxes especially in coastal zones where seawater pCO_2 varies over a wide range (e. g. 200–2000 μatm) [*Chavez and Takahashi*, 2007], and could have significant impact (up to a few ppm) on the atmospheric CO_2 concentration variation.

3.5. Contribution of Different Flux Components to CO_2 Variability

[25] To determine the relative importance of each flux component for successfully modeling synoptic variations in CO_2, we have separately correlated each CO_2 tracer with the observations. The resulting correlations and NSDs for separate flux components with respect to the measurement, averaged over all sites, are given in Table 3 and, averaged over groups of sites, are shown in Figure 7. The terrestrial biosphere flux component gives the largest contribution to the CO_2 synoptic variability (NSD), followed by the fossil fuel flux component. In most seasons the biospheric CO_2 also gives the largest correlation. With the exception of summer, the CASA-3hr flux component shows better correlations with the observations than the SiB-hr flux tracer. During the winter, SiB-hr flux produced NSD close to 1 so that with the addition of the FOS and OCN components the simulated CO_2 synoptic variability exceeded the observed variability by about 37%. On the other hand, FOS+OCN+CASA-3hr flux overestimated synoptic variability by ~24% during the spring. This difference between SiB-hr and CASA-3hr arises mainly from the continental sites, such as LEF (all three layers at 11, 76, and 244 m height). The oceanic flux component showed only marginal contributions to CO_2 synoptic variability, except for four remote sites (AMS, SMO, SPO, and SYO) where both the correlations and NSDs are of greater significance (Figure 7), mostly because of the small observed variability at remote locations. The OCN flux exhibits negative correlations during winter and spring at remote sites, and winter, spring and autumn at the mountain sites. The all-site average OCN correlation is less than half of those for FOS and BIO, and NSD captured is at about 16% of BIO and 26% of FOS. These fractions drop by another factor of two if the four sites with relatively high oceanic flux variability are excluded from the averaging.

[26] Figure 7 also demonstrates the relative importance of the time resolution in terrestrial biosphere fluxes. The improvement for the hourly versus monthly BIO tracers (noted earlier for LEF) is most evident in summer while in winter there is almost no difference. The negligible correlation for CASA-mon (CM) mainly arises from small negative correlations at HUN (two levels at 48 and 115 m height), NGL and MKW; at LEF (11 m) both CASA-mon and SiB-mon (SM) show negative correlations. All SiB fluxes produce small or negative correlations at the Continental sites during spring, possibly indicating poor timing of the onset of the growing season. This result is replicated at most of the Coastal sites (except ALT and YON) for both CASA and SiB fluxes. Overall, the tracer transport due to large-scale flow appears to be well modeled because the FOS flux component shows good correlations all year-round. This is also supported by consistently positive correlations for the OCN flux (lowest spatial heterogeneity among all fluxes) at continental and coastal sites (but note the very small NSD).

3.6. Dependence of Correlations on Model Resolution and Sampling Distance

[27] Three models (CCSR_NIES, TM3, and TM5 in subdomains) performed TransCom continuous simulations at two different horizontal resolutions with the same primary meteorology. A comparison of these results suggests that the model simulations at higher spatial resolution produce a better match with the observed CO_2 variations at most sites, particularly at WLG, DDR, AMY, SCH, CPT, and WES (not shown). The improvement in the model simulation

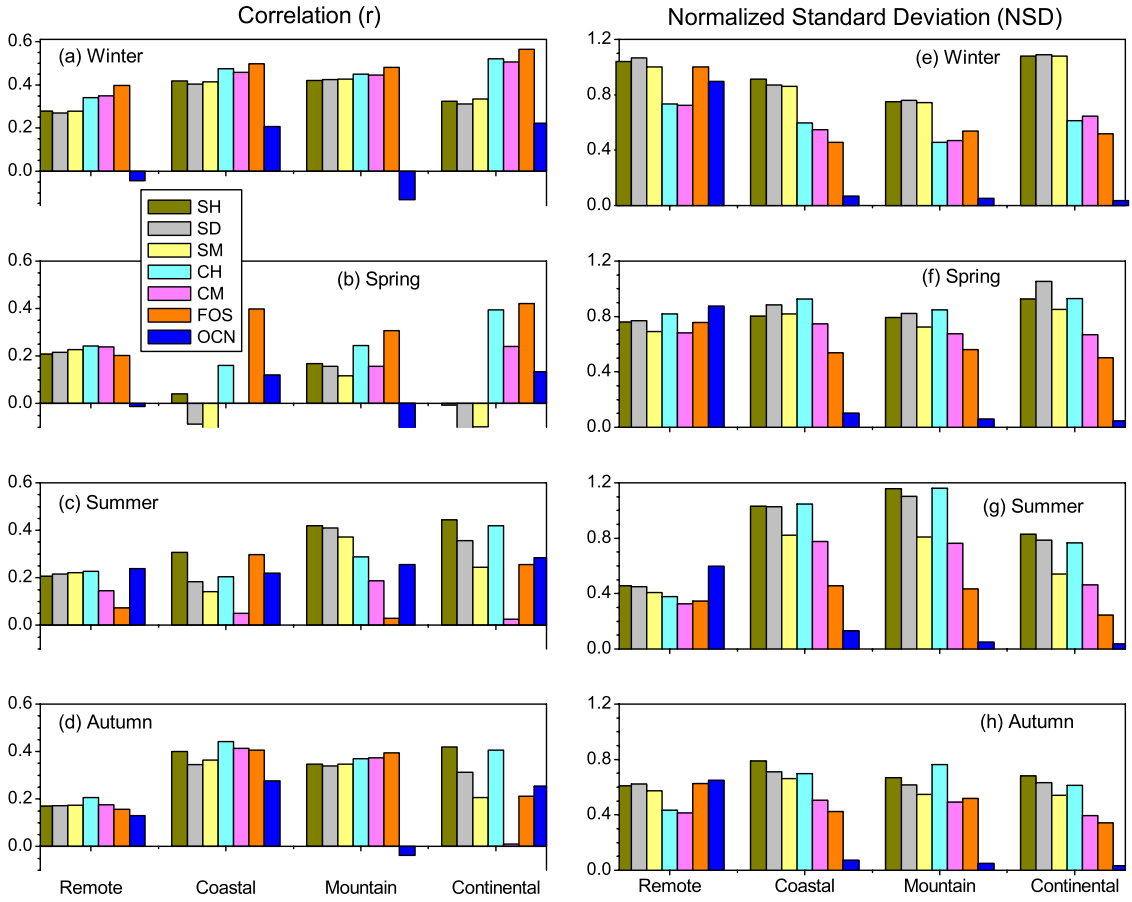

Figure 7. Histogram of averaged correlations (left) and NSDs (right) of simulated synoptic variations due to different CO_2 flux components (refer to Table 3 for legend abbreviations) and CO_2 data. The averaging is done over four seasons (as defined in the caption for Figure 6) and 20 global models (except IFS, which did not simulate SiB fluxes). Average observed SDs for (remote, coastal, mountain, and continental) site categories are (0.40, 4.41, 3.15, and 4.84 ppm), (0.36, 2.70, 2.59, and 4.37 ppm), (0.72, 3.22, 4.12, and 7.56 ppm), and (0.61, 4.19, 3.06, and 6.72 ppm) corresponding to winter, spring, summer, and autumn seasons, respectively.

could be due to a better representation of atmospheric transport, higher-resolution surface fluxes or sampling grid points closer to the true site location. To test which factor gives most improvement, we performed an extra model run (CCSR_NIES2lrf.FRCGC). This low-resolution flux (lrf) simulation case uses meteorological parameters identical to that in CCSR_NIES2 (T106) but the flux maps are interpolated from coarse (T42) resolution and hence are smoothed in their spatial patterns, but have identical magnitude of global total flux. Figure 8 shows a comparison of the correlations between simulated and observed daily CO_2 variations. The low-resolution flux run mostly gives similar results to the high-resolution flux indicating that the major improvements in correlations for the T106 run resulted from better representations of meteorology, terrain and sampling location compared to those in the T42 run. A contribution to the improved simulation from the resolution in surface fluxes can be seen at some sites, e.g., WLG, BHD, TKY, CPT, and CBW.

[28] To elucidate the role of model sampling location we estimated the distance between the model grid sampling location and the measurement location (in degrees) as

$$Sampling\_distance = \sqrt{(station\_lon - model\_lon)^2 + (station\_lat - model\_lat)^2} \quad (1)$$

[29] Generally, a larger correlation is obtained for smaller distances for most stations irrespective of the model, though this is more evident if only the models selecting nearest grid for sampling are considered (Figure 9). The TM5 models interpolated gridded model output to station locations ("zero" distance using equation (1)), but did not always produce the best correlation. Experiments with the TM5 model indicated that some stations were very sensitive to the sampling technique used (nearest grid, interpolation with the concentration slope or linear interpolation), and

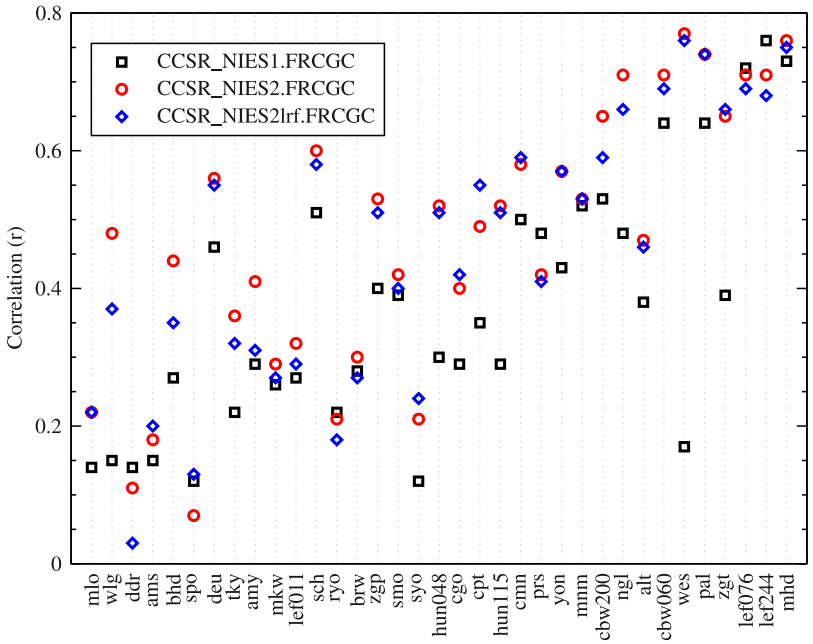

Figure 8. Correlation between modeled and observed daily average CO_2 for a low-resolution transport model with low-resolution fluxes (black symbols, CCSR_NIES1.FRCGC), high-resolution transport model with high-resolution fluxes (red symbols, CCSR_NIES2.FRCGC), and high-resolution model with low-resolution fluxes (blue symbols, CCSR_NIES2lrf.FRCGC). The results are shown for FOS+OCN+CASA-3hr flux simulations.

advantage of using a particular technique depends on the station location but no systematic differences were found. We found that the sampling distance has a much larger effect on the correlation between observed and modeled CO_2 variabilities at the continental and coastal sites (e.g., WES) compared to that for the remote stations (e.g., AMS) (Figure 9). This difference arises because of a more variable flux distribution around continental and coastal sites. Since the oceanic flux considered here has monthly mean and 4×5 degree intrinsic latitude-longitude resolution, sampling location error has minimal influence on determining CO_2 variability at the background stations. It is also worth noting that when a lower-resolution model (CCSR_NIES1) grid point is occasionally located closer to the site (e.g., LEF), compared to the grid point from its higher-resolution model version, higher correlation is obtained.

4. Conclusions

[30] We have compared daily averaged CO_2 concentrations from 25 transport model simulations with observations at 35 sites that have continuous monitoring. All time series

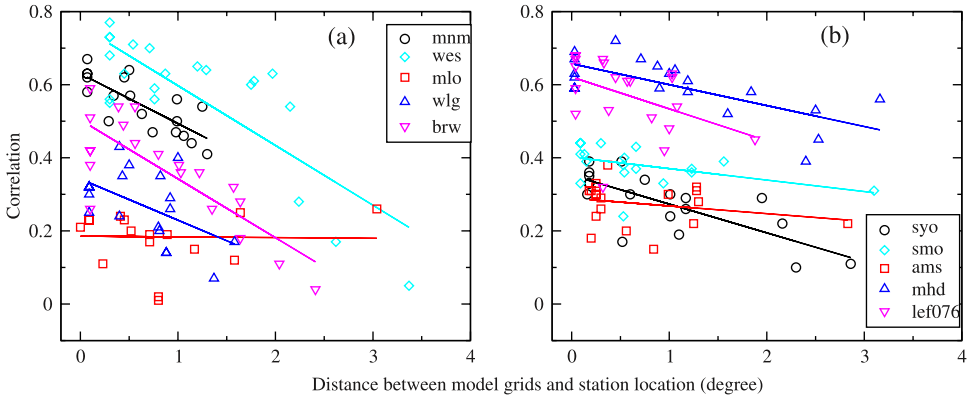

Figure 9. Correlations between modeled and observed daily CO_2 for all models (symbols) versus the sampling distance (equation (1)) for selected observation stations. The measurement stations are selected to represent all site types, e.g., continental (LEF), coastal (BRW, MHD, and WES), mountain (MLO and WLG), and remote (AMS, MNM, SMO, and SYO) and to depict clear evidence of strong versus negligible dependence of correlations on distance.

are passed through a digital filter to extract the synoptic variation component in the time series. All the models are able to capture some part of the synoptic variability consistently and the model skill varies for different location types, such as continental, mountain, coastal, and marine/remote. In general the models correlate better with each other than with the observations, indicating similarities in model transport. The major differences in model skills arise from the horizontal and vertical sampling locations corresponding to each model, and are fairly independent of the magnitude of observed variability at the sites. Both the representation of surface fluxes and transport model horizontal resolution has an observable impact on a model's ability to capture synoptic CO_2 variations, and their relative importance depends on whether the site is more influenced by surface fluxes or transport variability. Because of coarse vertical resolution in forward models, it is still challenging to identify the model levels that best represent mountain and tower data.

[31] The lead-lag correlations confirm that there is no systematic error in the model simulated timing of CO_2 peaks and troughs on synoptic timescales. Our analysis shows that the model ensemble average produces significantly improved correlations between the modeled and observed CO_2 time series compared to the average of individual transport models. Further analysis is needed to understand the improvements achieved in the case of the model ensemble compared to individual models. It would also be worthwhile to investigate alternative methods for generating a model ensemble using a single model, since most studies do not have the option of running multiple models. The correlation between observed and modeled synoptic variability and the relative amplitude of those variations were better simulated during winter than summer. The flux component analysis showed that under this experimental protocol, the terrestrial ecosystem flux is the most significant contributor to the CO_2 synoptic variability, followed by the fossil fuel emission with only a minor contribution due to the oceanic flux. Since we have used a large number of models in this analysis our overall conclusions are less biased toward specific model transport errors and therefore give more confidence in the following recommendations for future work.

[32] 1. Our analysis clearly reveals that increased horizontal resolution improves the simulation of synoptic-scale variations in CO_2. The match between observed and modeled variability is closely related to the distance between observing site location and model sampling grid as well as the improvement in model transport and representation of the surface fluxes. However, horizontal interpolation from the model grid to the site location does not always lead to an improvement in model-data comparison. Thus higher model resolution should be employed when possible. In addition, the use of a model ensemble is encouraged for better understanding the daily CO_2 variability.

[33] 2. There are some disagreements between terrestrial fluxes at similar time intervals obtained from CASA and SiB models at specific sites. However, the major conclusions of this study are not specific to the choice of terrestrial biospheric flux component (CASA-3hr or SiB-hr). There is also need for better temporal (~weekly or finer) and horizontal resolution (presently 4 × 5 degrees) in oceanic flux including interannual variability. This is suggested on the basis of the improvements in correlations and NSDs for the land site when diurnally varying terrestrial ecosystem fluxes are used compared to their monthly averages, and surprisingly low contribution of oceanic fluxes to synoptic-scale CO_2 variability at most sites.

[34] Data availability: The daily averaged and deseasonalized time series of modeled atmospheric CO_2 at these sites will be available online, in addition to the full TransCom continuous database. Information on how to access the data is available on the TransCom Web site (http://www.purdue.edu/transcom/T4_continuousSim.php).

[35] **Acknowledgments.** Maintaining continuous CO_2 observation records requires dedicated principal investigators, research teams and support staff. We wish to thank those who made their data available for this study. CO_2 measurements at many of the European locations including Hegyhatsal are sponsored by the CarboEurope project. Mace Head and Amsterdam Island CO_2 data is part of the ORE-RAMCES monitoring network coordinated by LSCE/IPSL and supported by INSU, CEA and IPEV. An experiment such as this generates a large model data set. Many thanks to Kevin Gurney and the Department of Earth and Atmospheric Sciences at Purdue University for data handling and ftp site hosting. We thank Cathy Trudinger for helpful comments on the manuscript. Suggestion from Philippe Peylin on correlations versus model resolution is appreciated. Individual modeling groups acknowledge the following support. CCAM: Part of this work was supported through the Australian Greenhouse Office. We thank John McGregor and Eva Kowalczyk for their development of CCAM. DEHM: Part of the work has been carried out within the CarboEurope-IP project funded by the European Commission. LLNL: The project (06-ERD-031) was funded by the Laboratory Directed Research and Development Program at LLNL. IFS: The work has been funded by EU's GEMS project SIP4-CT-2004-516099. CHIMERE is a model developed by IPSL, INERIS and LISA. Part of the implementation of CHIMERE-CO_2 has been supported through the French Environment and Energy Management Agency (ADEME) and the French Atomic Energy Commission (CEA). PKP is partly supported by the grants-in-aid for Creative Scientific Research (2005/17GS0203) of the Ministry of Education, Science, Sports and Culture, Japan; he wishes to thank Hajime Akimoto and Takakiyo Nakazawa for useful discussions and supporting this research at FRCGC. We sincerely thank the reviewers and associate editor James Randerson for providing critical comments to improve the quality of the article.

References

Baker, I. T., J. A. Berry, G. J. Collatz, A. S. Denning, N. P. Hanan, A. W. Philpott, L. Prihodko, K. M. Schaefer, R. S. Stockli, and N. S. Suits (2007), Global Net Ecosystem Exchange (NEE) fluxes of CO_2, ORNL Distrib. Active Arch. Cent., Oak Ridge, Tenn. (Available at http://www.daac.ornl.gov)

Bakwin, P. S., P. P. Tans, C. Zhao, W. Ussler, and E. Quesnell (1995), Measurements of carbon dioxide on a very tall tower, *Tellus, Ser. B*, *47*, 535–549.

Biraud, S., P. Ciais, M. Ramonet, P. Simmonds, V. Kazan, P. Monfray, S. O'Doherty, G. Spain, and S. G. Jennings (2002), Quantification of carbon dioxide, methane, nitrous oxide and chloroform emissions over Ireland from atmospheric observations at Mace Head, *Tellus, Ser. B*, *54*, 42–60.

Bregman, B., A. Segers, M. Krol, E. Meijer, and P. V. Velthoven (2003), On the use of mass-conserving wind fields in chemistry-transport models, *Atmos. Chem. Phys.*, *3*, 447–457.

Brunke, E.-G., C. Labuschagne, B. Parker, H. E. Scheel, and S. Whittlestone (2004), Baseline air mass selection at Cape Point, South Africa: Application of Rn-222 and other filter criteria to CO_2, *Atmos. Environ.*, *38*(33), 5693–5702, doi:10.1016/j.atmosenv.2004.04.024.

Chavez, F. P., and T. Takahashi (2007), Coastal oceans, in *The First State of the Carbon Cycle Report*, edited by A. W. King et al., chap. 15, pp. 131–140, SOCCR, Natl. Oceanic and Atmos. Admin., Natl. Clim. Data Cent., Asheville, N. C.

Conway, T. J., P. P. Tans, L. S. Waterman, K. W. Thoning, D. R. Kitzis, K. A. Masarie, and N. Zhang (1994), Evidence for interannual variability

of the carbon cycle from the National Oceanic and Atmospheric Administration/Climate Monitoring and Diagnostic Laboratory Global Air Sampling Network, *J. Geophys. Res.*, *99*, 22,831–22,855, doi:10.1029/94JD01951.

Corbin, K. D., A. S. Denning, L. Lu, J. Wang, and I. T. Baker (2008), Possible representation errors in inversions of satellite CO_2 retrievals, *J. Geophys. Res.*, *113*, D02301, doi:10.1029/2007JD008716.

Gaudry, A., P. Monfray, G. Polian, and G. Lambert (1990), Radon-calibrated emissions of CO_2 from South Africa, *Tellus, Ser. B*, *42*, 9–19, doi:10.1034/j.1600-0889.1990.00003.x.

Geels, C., S. Doney, R. Dargaville, J. Brandt, and J. H. Christensen (2004), Investigating the sources of synoptic variability in atmospheric CO_2 measurements over the Northern Hemisphere continents: A regional model study, *Tellus, Ser. B*, *56*, 35–50.

Geels, C., et al. (2007), Comparing atmospheric transport models for future regional inversions over Europe. Part 1: Mapping the CO_2 atmospheric signals, *Atmos. Chem. Phys.*, *7*, 3461–3479.

Gloor, M., P. Bakwin, D. Hurst, L. Lock, R. Draxler, and P. Tans (2001), What is the concentration footprint of a tall tower?, *J. Geophys. Res.*, *106*, 17,831–17,840, doi:10.1029/2001JD900021.

Gurney, K. R., et al. (2002), Towards robust regional estimates of CO_2 sources and sinks using atmospheric transport models, *Nature*, *415*, 626–630, doi:10.1038/415626a.

Haszpra, L. (2006), Atmospheric CO_2 hourly concentration data, Hegyhatsal (HUN), World Data Cent. for Greenhouse Gases, Japan Meteorol. Agency, Tokyo. (Available at http://gaw.kishou.go.jp/wdcgg.html)

Haszpra, L., Z. Barcza, P. S. Bakwin, B. W. Berger, K. J. Davis, and T. Weidinger (2001), Measuring system for the long-term monitoring of biosphere/atmosphere exchange of carbon dioxide, *J. Geophys. Res.*, *106*, 3057–3070, doi:10.1029/2000JD900600.

Hatakka, J. (2006), Atmospheric CO_2 hourly concentration data, Pallas, World Data Cent. for Greenhouse Gases, Japan Meteorol. Agency, Tokyo. (Available at http://gaw.kishou.go.jp/wdcgg.html)

Iwata, S. (2006), Atmospheric CO_2 hourly concentration data, Mikawa-Ichinomiya, World Data Cent. for Greenhouse Gases, Japan Meteorol. Agency, Tokyo. (Available at http://gaw.kishou.go.jp/wdcgg.html)

Karstens, U., M. Gloor, M. Heimann, and C. Rödenbeck (2006), Insights from simulations with high-resolution transport and process models on sampling of the atmosphere for constraining midlatitude land carbon sinks, *J. Geophys. Res.*, *111*, D12301, doi:10.1029/2005JD006278.

Kim, J.-S., and K.-J. Park (2006), Atmospheric CO_2 hourly concentration data, Anmyeon-do, World Data Cent. for Greenhouse Gases, Japan Meteorol. Agency, Tokyo. (Available at http://gaw.kishou.go.jp/wdcgg.html)

Langenfelds, R. L., R. J. Francey, B. C. Pak, L. P. Steele, J. Lloyd, C. M. Trudinger, and C. E. Allison (2002), Interannual growth rate variations of atmospheric CO_2 and its $\delta^{13}C$, H_2, CH_4, and CO between 1992 and 1999 linked to biomass burning, *Global Biogeochem. Cycles*, *16*(3), 1048, doi:10.1029/2001GB001466.

Law, R. M., et al. (1996), variations in modeled atmospheric transport of carbon dioxide and the consequences for CO_2 inversions, *Global Biogeochem. Cycles*, *10*, 783–796, doi:10.1029/96GB01892.

Law, R. M., P. J. Rayner, L. P. Steele, and I. G. Enting (2002), Using high temporal frequency data for CO_2 inversions, *Global Biogeochem. Cycles*, *16*(4), 1053, doi:10.1029/2001GB001593.

Law, R. M., P. J. Rayner, and Y. P. Wang (2004), Inversion of diurnally varying synthetic CO_2: Network optimization for an Australian test case, *Global Biogeochem. Cycles*, *18*, GB1044, doi:10.1029/2003GB002136.

Law, R. M., W. Peters, and C. R. Rödenbeck (2006), TransCom continuous experimental protocol, technical report, 17 pp., Purdue Clim. Cent., Purdue Univ., Lafayette, Ind. (Available at http://www.purdue.edu/transcom/T4_continuousSim.php)

Law, R. M., et al. (2008), TransCom model simulations of hourly atmospheric CO_2: Experimental overview and diurnal cycle results for 2002, *Global Biogeochem. Cycles*, *22*, GB3009, doi:10.1029/2007GB003050.

Martinotti, V., F. Apadula, and C. Vannini (2006), Atmospheric CO_2 hourly concentration data, Plateau Rosa, World Data Cent. for Greenhouse Gases, Japan Meteorol. Agency, Tokyo. (Available at http://gaw.kishou.go.jp/wdcgg.html)

Morimoto, S., T. Nakazawa, K. Higuchi, and S. Aoki (2000), Latitudinal distribution of atmospheric CO_2 sources and sinks inferred by ^{13}C: Measurements from 1985 to 1991, *J. Geophys. Res.*, *105*, 24,315–24,326, doi:10.1029/2000JD900386.

Murayama, S., S. Yamamoto, N. Saigusa, and H. Kondo (2006), Atmospheric CO_2 hourly concentration data, Takayama, World Data Cent. for Greenhouse Gases, Japan Meteorol. Agency, Tokyo. (Available at http://gaw.kishou.go.jp/wdcgg.html)

Muto, Y. (2006), Atmospheric CO_2 hourly concentration data, Mt. Dodaira, World Data Cent. for Greenhouse Gases, Japan Meteorol. Agency, Tokyo. (Available at http://gaw.kishou.go.jp/wdcgg.html)

Nakazawa, T., M. Ishizawa, K. Higuchi, and N. B. A. Trivett (1997), Two curve fitting methods applied to CO_2 flask data, *Environmetrics*, *8*, 197–218, doi:10.1002/(SICI)1099-095X(199705)8:3<197::AID-ENV248>3.0.CO;2-C.

Olivier, J. G. J., and J. J. M. Berdowski (2001), Global emissions sources and sinks, in *The Climate System*, edited by J. Berdowski, R. Guicherit, and B. J. Heij, pp. 33–78, A. A. Balkema Publ., Lisse, Netherlands, ISBN:9058092550.

Olsen, S. C., and J. T. Randerson (2004), Differences between surface and column atmospheric CO_2 and implications for carbon cycle research, *J. Geophys. Res.*, *109*, D02301, doi:10.1029/2003JD003968.

Patra, P. K., S. Maksyutov, M. Ishizawa, T. Nakazawa, T. Takahashi, and J. Ukita (2005), Interannual and decadal changes in the sea-air CO_2 flux from atmospheric CO_2 inverse modelling, *Global Biogeochem. Cycles*, *19*, GB4013, doi:10.1029/2004GB002257.

Peters, W., J. B. Miller, J. Whitaker, A. S. Denning, A. Hirsch, M. C. Krol, D. Zupanski, L. Bruhwiler, and P. P. Tans (2005), An ensemble data assimilation system to estimate CO_2 surface fluxes from atmospheric trace gas observations, *J. Geophys. Res.*, *110*, D24304, doi:10.1029/2005JD006157.

Peylin, P., P. J. Rayner, P. Bousquet, C. Carouge, F. Hourdin, P. Heinrich, P. Ciais, and AEROCARB contributors (2005), Daily CO_2 flux estimates over Europe from continuous atmospheric measurements: 1. Inverse methodology, *Atmos. Chem. Phys.*, *5*, 3173–3186.

Randerson, J. T., M. V. Thompson, T. J. Conway, I. Y. Fung, and C. B. Field (1997), The contribution of terrestrial source and sinks to trends in the seasonal cycle of atmospheric carbon dioxide, *Global Biogeochem. Cycles*, *11*, 535–560, doi:10.1029/97GB02268.

Rödenbeck, C. (2005), Estimating CO_2 sources and sinks from atmospheric mixing ratio measurements using a global inversion of atmospheric transport, *Max-Planck-Inst. für Biogeochem. Tech. Rep. 6*, 53 pp., Jena, Germany. (Available at http://www.bgc-jena.mpg.de)

Rödenbeck, C., S. Houweling, M. Gloor, and M. Heimann (2003), CO_2 flux history 1982–2001 inferred from atmospheric data using a global inversion of atmospheric transport, *Atmos. Chem. Phys.*, *3*, 1919–1964.

Russell, G. L., and J. A. Lerner (1981), A new finite-differencing scheme for the tracer transport equation, *J. Appl. Meteorol.*, *20*, 1483–1498, doi:10.1175/1520-0450(1981)020<1483:ANFDSF>2.0.CO;2.

Sasaki, H. (2006), Atmospheric CO_2 hourly concentration data, Minamitorishima, Ryori and Yonagunijima, World Data Cent. for Greenhouse Gases, Japan Meteorol. Agency, Tokyo. (Available at http://gaw.kishou.go.jp/wdcgg.html)

Takahashi, T., et al. (2002), Global sea-air CO_2 flux based on climatological surface ocean pCO_2, and seasonal biological and temperature effects, *Deep Sea Res., Part II*, *49*, 1601–1622, doi:10.1016/S0967-0645(02)00003-6.

Taylor, K. E. (2001), Summarizing multiple aspects of model performance in single diagram, *J. Geophys. Res.*, *106*, 7183–7192, doi:10.1029/2000JD900719.

Tsutsumi, Y., K. Mori, M. Ikegami, T. Tashiro, and K. Tsuboi (2006), Long-term trends of greenhouse gases in regional and background events observed during 1998–2004 at Yonagunijima located to the east of the Asian continent, *Atmos. Environ.*, *40*, 5868–5879, doi:10.1016/j.atmosenv.2006.04.036.

Uhse, K., F. Meinhardt, and L. Ries (2006), Atmospheric CO_2 hourly concentration data, Deuselbach, Neuglobsow, Schauinsland, Westerland, Zingst, Zugspitze/Schneefernerhaus, World Data Cent. for Greenhouse Gases, Japan Meteorol. Agency, Tokyo, Air Monit. Network of the Fed. Environ. Agency. (Available at http://gaw.kishou.go.jp/wdcgg.html)

Wada, A., Y. Sawa, H. Matsueda, S. Taguchi, S. Murayama, S. Okubo, and Y. Tsutsumi (2007), Influence of continental air mass transport on atmospheric CO_2 in the western North Pacific, *J. Geophys. Res.*, *112*, D07311, doi:10.1029/2006JD007552.

Wang, J.-W., A. S. Denning, L. Lu, I. T. Baker, K. D. Corbin, and K. J. Davis (2007), Observations and simulations of synoptic, regional, and local variations in atmospheric CO_2, *J. Geophys. Res.*, *112*, D04108, doi:10.1029/2006JD007410.

Zhou, L., J. Tang, Y. P. Wen, J. L. Li, P. Yan, and X. C. Zhang (2003), The impact of local winds and long-range transport on the continuous carbon dioxide record at Mount Waliguan, China, *Tellus, Ser. B*, *55*, 145–158.

C. Aulagnier, P. Bousquet, F. Delage, L. Rivier, and R. Vautard, Laboratoire des Sciences du Climat et de l'Environnement, IPSL, CEA Saclay, UVSQ, CNRS, Orme des Merisiers, Bat. 701, F-91191 Gif sur

Yvette CEDEX, France. (celine.aulagnier@lsce.ipsl.fr; philippe.bousquet@lsce.ipsl.fr; francois.delage@cea.fr; leonard.rivier@lsce.ipsl.fr; robert.vautard@cea.fr)

I. Baker, A. S. Denning, R. Lokupitiya, and N. Parazoo, Department of Atmospheric Science, Colorado State University, Fort Collins, CO 80523, USA. (baker@atmos.colostate.edu; denning@atmos.colostate.edu; ravi@atmos.colostate.edu; nparazoo@atmos.colostate.edu)

D. J. Bergmann and P. J. Cameron-Smith, Lawrence Livermore National Laboratory, 7000 East Avenue (L-103), Livermore, CA 94550, USA. (dbergmann@llnl.gov; pjc@llnl.gov)

J. Brandt, J. H. Christensen, and C. Geels, National Environmental Research Institute, Department of Atmospheric Environment, University of Aarhus, Frederiksborgvej 399, P.O. Box 358, DK-4000 Roskilde, Denmark. (jbr@dmu.dk; jc@dmu.dk; cag@dmu.dk)

L. Bruhwiler, NOAA/ESRL/GMD, 325 Broadway, Boulder, CO 80305-3337, USA. (lori.bruhwiler@noaa.gov)

S. Fan and S.-J. Lin, NOAA/Geophysical Fluid Dynamics Laboratory, P.O. Box 308, 201 Forrestal Road, Princeton, NJ 08542-0308, USA. (songmiao.fan@noaa.gov; shian-jiann.lin@noaa.gov)

S. Houweling, Netherlands Institute for Space Research, Sorbonnelaan 2, NL-3584 CA Utrecht, Netherlands. (s.houweling@phys.uu.nl)

R. Imasu, Y. Niwa, and M. Satoh, Center for Climate System Research, University of Tokyo, 5-1-5 Kashiwanoha, Kashiwa-shi, Chiba 277-8568, Japan. (imasu@ccsr.u-tokyo.ac.jp; yniwa@ccsr.u-tokyo.ac.jp; satoh@ccsr.u-tokyo.ac.jp)

U. Karstens and C. Rödenbeck, Max-Planck-Institute for Biogeochemistry, P.O. Box 10 01 64, D-07701 Jena, Germany. (ute.karstens@zmaw.de; christian.roedenbeck@bgc-jena.mpg.de)

S. R. Kawa, NASA Goddard Space Flight Center, Code 613.3, Greenbelt, MD 20771, USA. (stephan.r.kawa@nasa.gov)

J. Kleist, Privacy Networks, 200 W. Mountain Avenue, Suite 102, Fort Collins, CO 80521, USA. (johnk@privacynetwork.com)

M. C. Krol, IMAU/SRON, University Utrecht, Princetonplein 5, NL-3584 CC, Utrecht, Netherlands. (m.c.krol@phys.uu.nl)

R. M. Law, CSIRO Marine and Atmospheric Research, PMB 1, Aspendale, Vic 3195, Australia. (rachel.law@csiro.au)

T. Maki, Atmospheric Environment Division, Japan Meteorological Agency, 1-3-4 Otemachi, Chiyoda-ku, Tokyo 100-8122, Japan. (maki@met.kishou.go.jp)

S. Maksyutov, Center for Global Environmental Research, National Institute for Environmental Studies, 16-2 Onogawa, Tsukuba, Ibaraki 305-8506, Japan. (shamil@nies.go.jp)

R. Onishi, Earth Simulator Center, JAMSTEC, 3173-25 Showa-machi, Kanazawa-ku, Yokohama 236-0001, Japan. (onishi.ryo@jamstec.go.jp)

P. K. Patra and M. Takigawa, Frontier Research Center for Global Change, JAMSTEC, 3173-25 Showa-machi, Kanazawa-ku, Yokohama 236-0001, Japan. (prabir@jamstec.go.jp; takigawa@jamstec.go.jp)

W. Peters, Department of Meteorology and Air Quality, Wageningen University and Research Center, Droevendaalsesteeg 4, NL-6708 PB Wageningen, Netherlands. (wouter.peters@wur.nl)

G. Pieterse, TNO Science and Industry, De Rondom 1, NL-5612 AP Eindhoven, Netherlands. (gerben.pieterse@tno.nl)

S. Serrar, ECMWF, Shinfield Park, Reading RG2 9AX, UK. (soumia.serrar@ecmwf.int)

S. Taguchi, National Institute of Advanced Industrial Science and Technology, AIST-West, 16-1 Onogawa, Tsukuba, Ibaraki 305-8569, Japan. (s.taguchi@aist.go.jp)

A. T. Vermeulen, Energy Research Centre of the Netherlands, P.O. Box 1, NL-1755 ZG Petten, Netherlands. (a.vermeulen@ecn.nl)

Z. Zhu, Science Systems and Applications Incorporated, 10210 Greenbelt Road, Suite 600, Lanham, MD 20706, USA. (zhu@mulan.gsfc.nasa.gov)